Advanced Ceramics Progress: Vol. 6, No. 4, (Autumn 2020) 15-21

Advanced Ceramics Progress

Research Article

Journal Homepage: www.acerp.ir

Effect of Heat Treatment on Grain Growth of Magnetic Nanocrystalline Hydroxyapatite Powder

S. Kouhkanzadeh [a], I. Mobasherpour [a] *, M. J. Molaei [b], E. Salahi [a], M. Pazouki [c]

[a] *Department of Ceramic, Materials and Energy Research Center, Meshkindasht, Alborz, Iran*
[b] *Faculty of Chemical and Materials Engineering, Shahrood University of Technology, Shahrood, Semnan, Iran*
[c] *Department of Energy, Materials and Energy Research Center, Meshkindasht, Alborz, Iran*

ARTICLE INFO

Article History:

Received 3 August 2020
Received in revised form 1 November 2020
Accepted 4 November 2020

Keywords:

Magnetic Hydroxyapatite
Nanostructure
Crystal Growth
Activation Energy

ABSTRACT

Nanocrystalline Magnetic Hydroxyapatite (MHAp) was synthesized through co-precipitation method and the subsequent heat treatment. Phase analysis, particle morphology, chemical bonding, and magnetic properties were studied using XRD, FESEM, FTIR, and VSM, respectively. The XRD results showed that MHAp was formed by heat treatment at 1100 °C. The samples heat-treated at 500 and 1100 °C incorporated a plate-like morphology with a mean crystallite size of 11.7 and 59.9 nm, respectively. In addition, the VSM results indicated that the synthesized MHAp was characterized by magnetic features after heat treatment. According to the findings in this study, the coercive field (H_c), saturation magnetization (M_s), and magnetism stayed (M_r) were 0.175 kO_e, 0.00147, and 0.02615 $emug^{-1}$, respectively, in -10 to 10 kO_e magnetic field. The growth kinetics of the MHAp was alo studied. According to the results, the growth activation energies for low and high temperatures were 45.51 and 67.33 kJ/mol, respectively. Owing to several properties already proven, the MHAp powder was successfully synthesized.

https://doi.org/10.30501/acp.2020.241694.1040

1. INTRODUCTION

Apatite-group minerals are of great economic and scientific significance due to their low cost, availability, and ease of use [1]. HAp is a mineral that consists of phosphate and calcium which can be found in animal and human hard tissues such as mammalian teeth, vertebrate bones, mature teeth of some chiton species, and fish scales [2]. HAp with the space group of P63/m, has a hexagonal crystal structure. The unit cell of the HAp consists of six PO_4^{3-}, ten Ca^{2+}, and two OH^-. The ion exchange strength of metal ions with Ca^{2+} makes HAp capable of immobilizing the heavy metal ions in water sources [3]. Apatite can be produced by a co-precipitation synthesis method using phosphate and calcium. HAp with the chemical formula of $Ca_{10}(PO_4)_6(OH)_2$-A has been extensively used for removing the contaminants from aqueous solutions [1]. The HAp is also efficient in the removal of different heavy metal ions such as lead, cadmium, copper, nickel, zinc, uranium, and cobalt from aqueous solutions. This material enjoys several advantages including low solubility in water, good buffering characteristics, and high stability during oxidation, making it a promising substance for the recovery of the heavy metal ions from aqueous solutions [4].

Utilization of magnetic nanoparticles in different applications such as wastewater treatment, biomedical, and catalyst support has been extensively investigated in recent years. Among the magnetic nanoparticles, magnetic HAp has attracted considerable attention due to its excellent metal ions adsorption, hyperthermia characteristics, biocompatibility, low cost, and eco-friendliness [5]. The synthesis of iron oxides and HAp

* Corresponding Author Email: iman.mobasherpour@gmail.com (I. Mobasherpour) URL: http://www.acerp.ir/article_121661.html

Please cite this article as: Kouhkanzadeh, S., Mobasherpour, I., Molaei, M. J., Salahi, E., Pazouki, M., "Effect of Heat treatment on Grain Growth of Magnetic Nanocrystalline Hydroxyapatite Powder", ***Advanced Ceramics Progress***, Vol. 6, No. 4, (2020), 15-21

nanoparticles have been thoroughly investigated by several researchers worldwide. However, investigation of the synthesis of magnetic HAp is limited to fewer studies [6]. Different synthesis routes were employed to produce the magnetic HAp. It can be synthesized by the substitution of transition metal ions into the HAp crystal structure. It was observed that the substitution of Fe^{2+}, Co^{2+}, and Mn^{2+} ions into the crystal structure of the HAp would result in the magnetic moments of 4, 3, and 5 Bohr magnetons, respectively [7]. The magnetic HAp can also be synthesized by making composites of magnetic materials and HAp. Different magnetic nanoparticles such as Fe_3O_4 [8-11], $MgFe_2O_4$ [12], $CoFe_2O_4$ [13], $NiFe_2O_4$ [14], and $ZnFe_2O_4$ [15] were utilized to synthesize the magnetic HAp. Different synthesis methods were also employed to produce the magnetic HAp including microwave-assisted route [16], mechano-chemical [17], precipitation followed by hydrothermal [18], and co-precipitation [1].

The present study aims to synthesize the magnetic HAp through the co-precipitation method. The effect of heat treatment temperature on phase composition was also investigated. In addition, the grains growth kinetics was explored. Moreover, the growth constants and activation energy of the growth were obtained.

2. MATERIALS AND METHODS

2.1. Materials

Ferric chloride hexahydrate ($FeCl_3.6H_2O$, Merck Art no. 231-729-4), iron (II) chloride tetrahydrate ($FeCl_2.4H_2O$, Merck Art no. 231-843-4), diammonium hydrogen phosphate ($(NH_4)_2HPO_4$, Merck Art no. 231-987-8), calcium nitrate ($Ca(NO_3)_2$, Merck Art no. 233-332-1), and Ammonia solution 25% (NH_4OH, Merck Art no. 1054321000) were used in the present study without further purifications. All of the prepared solutions were used without storage time. All glassware was rinsed with distilled water and dried before use.

2.2. Preparation of magnetic HAp nanoparticles

Synthesis of the magnetic HAp nanoparticles was performed through the co-precipitation method. First, 0.4107, 1.1057, 8.96, and 23.81 gr of ferrous chloride, ferric chloride, diammonium hydrogen phosphate, and calcium nitrate were weighed, respectively. Ferrous chloride and ferric chloride were added to 30 ml distilled water and mixed in 30 minutes. At the same time, calcium nitrate and diammonium hydrogen phosphate were added to 250 ml distilled water and mixed in 30 minutes. After the preparation of the solutions, Iron chloride and calcium nitrate solutions were added and mixed together. The mixture was stirred for 5 minutes. In the next step, diammonium hydrogen phosphate solution was added as the same time as NH_4OH was used to adjuste pH 11 at room temperature. By adding NH_4OH, the color of the initial solution turned from light brown to black. Each uncolored drop of diammonium hydrogen phosphate turned white by dropping into the black solution that finally changed the whole solution color. Th final solution rested for 24 hours. After rest, the light brown sediment was deposited at the end of the balloon which was covered by uncolored liquid. Sediment was separated by centrifuge at 4000 rpm for 10 minute and was dried in oven for 24h at 90°C. The process was followed by heat treatment at 500, 700, 900, and 1100°C, and, 1100°C for an hour in a tube furnace. Total heat treatment time was 3 hours with a heating rate of 10 K/min.

2.3. Instrumentation

Synthesized powders were analyzed by X-Ray Diffraction (XRD) (Siemens D-500, Cu-K_α radiation λ=1.54 A°, 30KV. in Bragg- Brentano geometry (θ-2θ)), one of the most exclusive equipment used for analysis and specific determination of crystals properties such as diagnosis of the phases, size and, distance among the crystalline layers in crystals. During the heat treatment, phase transformations and change in the size of crystals were expected and the extent of these changes was estimated using the XRD results and Scherrer method [19]:

$$t = \frac{0.9\lambda}{B\cos\theta} \quad (1)$$

where (t) is the average crystallite size (nm), λ is the CuKα wave length (nm), B is the diffraction peak width in a half maximum intensity (radian), and θ is the Bragg diffraction angle.

Samples were sent for Fourier Transform Infrared Spectroscopy (FT-IR) test to characterize the composition and confirm the XRD results. The FT-IR test was performed by Bruker's infrared vector 33 spectroscopy device in the range of 4000-400 cm^{-1} of wavenumber. Synthesized MHAp was observed by SEM (MIRA3TEScan, HV: 15.0 KV). The magnetic properties were checked by Vibrating Sample Magnetometer (VSM) (Magnetic Daghigh Kavir type MDKB) that operates based on Faraday's imposing law.

3. RESULTS AND DISCUSSION

3.1. Characterization of MHAp

Fig. 1 compares the results obtained from X-ray test of heat treatment powders at different temperatures of 500, 700, 900, and 1100°C for 1 hour by Xpert software. As observed, the amorphous magnetite hydroxyapatite phase was formed at the lowest temperature of the heating process. Heat treatment at 700°C revealed the same result as 500°C. At a temperature of 900°C, Tri-Calcium Phosphate (TCP) phase was formed in the presence of the MHAp phase. The presence of the iron element in the environment system reduced the decomposition temperature of the hydroxyapatite to the TCP phase [20]. Increasing the temperature of the system led to an increase in the intensity peak of tricalcium phosphate. The peaks shown in the MHAp and TCP phases in 1100°C were sharper mainly due to theirs higher degrees of crystallization. On the contrary, at 1100°C, the graph moved slightly to the left due to the presence of iron at the site of the cations in the hydroxyapatite structure. Finally, the results of the sample heated at 1100°C temperature for an hour showed that a majority of the hydroxyapatite markers in other samples were converted to tricalcium phosphate, indicating a phase transformation and excessive decomposition of hydroxyapatite to tricalcium phosphate at this temperature.

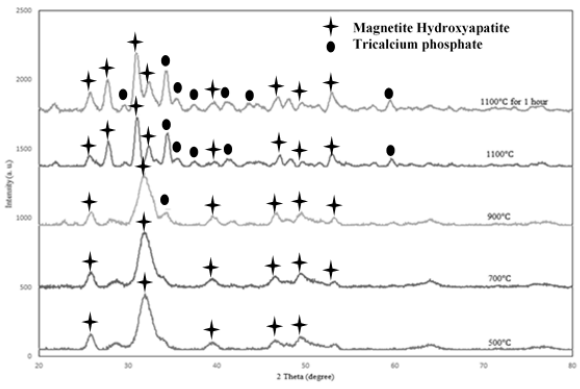

Figure 1. XRD results of the heat treatment magnetic hydroxyapatite powders at 500, 700, 900, 1100, and 1100°C for 1 hour

In Table 1, the crystallite size of MHAp as a function of heat treatment based on the XRD profile analysis were shown. To calculate the size of crystals, a method based on Scherrer's method and an expert software were employed. It was observed that as temperature increased from 500°C up to 1100°C, the crystallite size of magnetic hydroxyapatite increased.

TABLE 1. The crystallite size of MHAp crystalline as a function of heat treatment

No.	Temperature [°C]	Crystallite size [nm]
1.	500	11.70
2.	700	18.70
3.	900	32.90
4.	1100	59.90

Examination of FT-IR powder test results is also an affirmation for XRD results. In the infrared spectroscopic spectrum, a series of absorption bands were observed in the middle region of infrared waves. As illustrated in Fig. 2, the adsorption band 1043 cm^{-1} represents the P-O bond [21]. Although sharp peaks such as 548 and 607 cm^{-1} indicate O-P-O bond in hydroxyapatite [22], peak 548 cm^{-1} represents Fe-O bond in Hydroxyapatite structure [23]. The peak ranges of 887, 919, and 1043 cm^{-1} show the P-O bond, and the peak of 3423 cm^{-1} represents O-H bond in this composition [21].

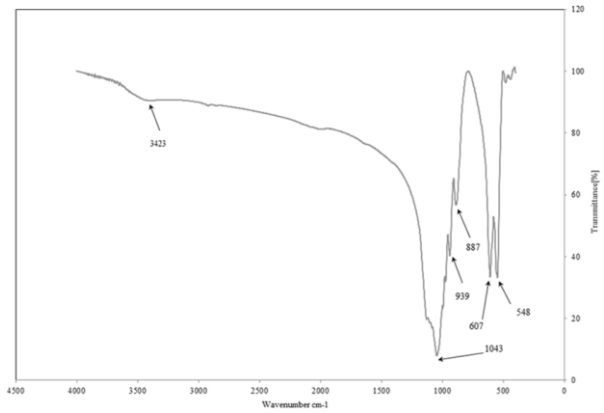

Figure 2. FT-IR pattern of MHAp heated at 1100°C

Fig. 3 indicates the FE-SEM pictures of magnetic hydroxyapatite powder heated at 500℃ and 1100℃. According to the pictures, the crystals of MHAp grow during the heating process. The results obtained from FE-SEM test were in agreement with those of the XRD test in Scherrer's method. The morphology of the particles in the (a) and (b) images are in the form of Irregular flat.

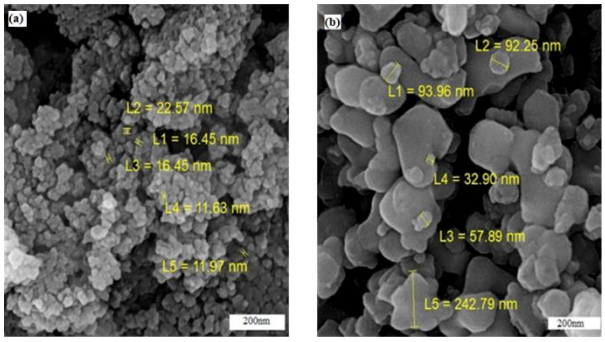

Figure 3. FE-SEM pictures of the MHAp powder heated at 500℃ (a) and 1100℃ (b)

3.2. Investigation of magnetic properties

The sample heated at 1100℃ was the main sample used for VSM test. According to Fig. 4 and its hysteresis loop, coercive field (H_c), saturation magnetization (M_s), and magnetism stayed (M_r) are 0.175 kO_e, 0.00147 $emug^{-1}$, and 0.02615 $emug^{-1}$, respectively, in -10 to 10 kO_e magnetic field. Based on the obtained numbers and slope of the hysteresis curve, it can be concluded that the MHAp was characterized by a low magnetic property. The formation of low saturation magnetic field can be due to the interaction of diamagnetic reaction of hydroxyapatite with magnetite particles. In other words, applying a magnetic field to the MHAp powder creates an induced magnetic field in an opposite direction to the applied field in the structure, which can reduce the magnetic strength of the powder [24].

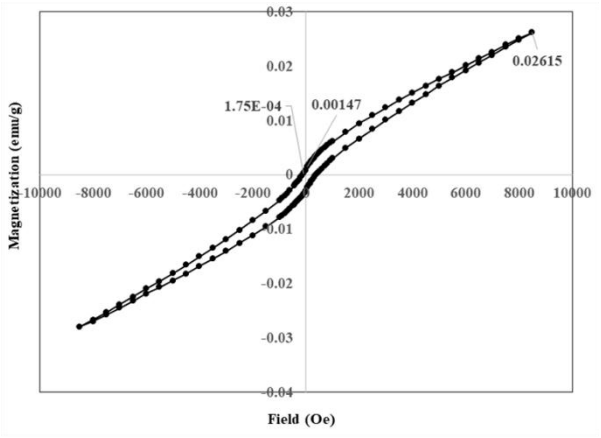

Figure 4. Hysteresis loop of MHAp heated in 1100°C by VSM test

3.3. Investigation of grain growth

According to the results presented in Table 1, during heat treatment, nanoscale grain growth occurs. In general, grain growth occurs in polycrystalline materials to decrease the free energy of the system by reducing the total grain boundary energy. The earliest consideration of kinetics of normal grain growth assumes a liner relation between the growth rate and the inverse of crystallite size [25, 26]:

$$\frac{dD}{dt} = \frac{k}{D} \tag{2}$$

where D, t, and k are the main grain diameter, heating time, and growth rate constant, respectively. The integration form of this equation is:

$$D^2 - D_0^2 = kt \tag{3}$$

And

$$k = k_0 exp\left(-\frac{Q}{RT}\right) \tag{4}$$

where R, Q, T, and k_0 are the universal gas constant, activation energy, absolute temperature, and a constant, respectively. Equations (3) and (4) are used for a simple investigation of the growth rate and activation energy of MHAp crystallites. Approximately, a single growth process can be separated as several domains where k is the constant for each domain [27]:

$$\int_{D_0}^{D_n} DdD = \int_{D_0}^{D_1} DdD + \cdots + \int_{D_{n-1}}^{D_n} DdD = \int_{t_0}^{t_1} k_1 dt + \cdots + \int_{t_{n-1}}^{t_n} k_n dt \tag{5}$$

Or

$$D^2 - D_0^2 = \begin{Bmatrix} k_1 t & t \le t_1 \\ \cdots & \cdots \\ k_1 t + \cdots + k_n (t_n - t_{n-1}) & t_n > t > t_{n-1} \end{Bmatrix} \tag{6}$$

k_1, k_2, …, and k_n are the growth rate constants in each domain. The values for k_1, k_2, and k_3 for n=3 were calculated in this study, the results of which are presented in Table 2 and Fig. 5. As mentioned earlier, the growth rate constants increase with time: $k_1 < k_2 < k_3$. The activation energy can be obtained from Equation (4) as the slope of a plot of (ln k) against (1/T). This plot is shown in Fig. 6 for the minor and major temperatures of every domain. The average activation energies for lower and higher temperatures are 45.51 and 67.33 kJ/mol, respectively.

TABLE 2. Constant growth rate in each domain

Time range [s]	Rate constant $[nm^2/s]$
3000-4200	0.1773
4200-5400	0.6106
5400-6600	2.0482

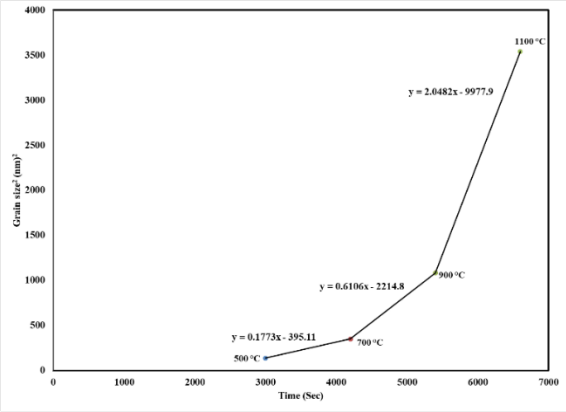

Figure 5. Growth curve based on time of MHAp for n=3 according to Equation 6

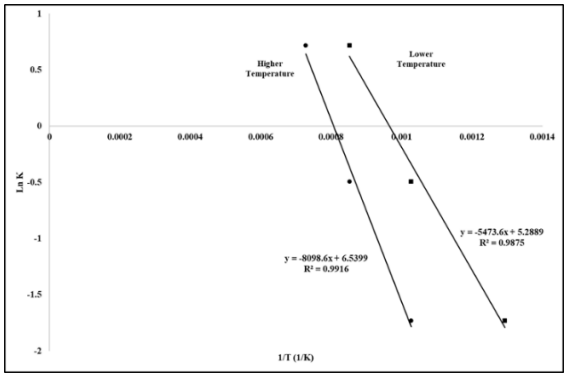

Figure 6. Arrhenius plot of logarithm of the rate constants versus reciprocal heat treatment temperature

Of note, for nanoscale materials, the grain growth was accompanied by a reduction in the diffusion rate and increase in the activation energy of diffusion [28]. It is unclear what happens in the growth process of MHAp during heat treatment. F. Liu and R. Kirchheim [29] introduced a new empirical relationship using the Gibbs adsorption equation and McLean model for grain boundary segregation. According to this approach, in systems with high segregation energy, decreasing the grain boundary energy to zero is possible. In addition, the decrease in the activation energy can be described through this equation. The crystallite size is proportional to the inverse exponential part of temperature with in their relation [30]:

$$D = \frac{A}{B - exp\left(-\frac{C}{T}\right)} \quad (7)$$

where A, B, and C are constant coefficients and T is temperature. Relationship (7) can present a better fitting for the MHAp growth profile. Of note, at high temperature (about 1673 K), the H and O atoms leave HAp crystalline lattice, and this defect in the lattice facilitates the formation of tricalcium phosphate. According to F. Liu and R. Kirchheim, the mobility of H and O atoms may increase at high temperatures, making the crystallites overcome the energy barrier at the grain boundary. This can be described as a "semi-segregation" phenomenon during heat treatment and explains changes in the rate constant and activation energy at high temperatures. It should be noted that the constants in the F. Liu and R. Kirchheim relation are not known for MHAp [30].

4. CONCLUSION

The VSM results showed that the synthesized MHAp had magnetic characteristics after heat treatment. In this study, the coercive field (H_c), saturation magnetization (M_s), and magnetism stayed (M_r) were 0.175 kOe, 0.00147 $emug^{-1}$, and 0.02615 $emug^{-1}$, respectively, in -10 to 10 kO_e magnetic field. The growth kinetics of the magnetic HAp crystallite was also studied. The results revealed the growth activation energies of 45.51 and 67.33 kJ/mol for low- and high-temperature ranges, respectively. Due to the properties which has been proven eralier, the MHAp powder was successfully synthesized.

5. ACKNOWLEDGMENTS

The authors would like to acknowledge the financial support of Materials & Energy Research Center of Iran for this research.

REFERENCES

1. Thanh, D. N., Novák, P., Vejpravova, J., Vu, H. N., Lederer, J., Munshi, T., "Removal of copper and nickel from water using nanocomposite of magnetic hydroxyapatite nanorods", ***Journal***

of Magnetism and Magnetic Materials, Vol. 456, (2018), 451-460. https://doi.org/10.1016/j.jmmm.2017.11.064

2. Ramdani, A., Kadeche, A., Adjdir, M., Taleb, Z., Ikhou, D., Taleb, S., Deratani, A., "Lead and cadmium removal by adsorption process using hydroxyapatite porous materials", ***Water Practice & Technology***, Vol. 15, No. 1, (2020), 130-141. https://doi.org/10.2166/wpt.2020.003
3. Wang, Y., Hu, L., Zhang, G., Yan, T., Yan, L., Wei, Q., Du, B., "Removal of Pb (II) and methylene blue from aqueous solution by magnetic hydroxyapatite-immobilized oxidized multi-walled carbon nanotubes", ***Journal of Colloid and Interface Science***, Vol 494, (2017), 380-388. https://doi.org/10.1016/j.jcis.2017.01.105
4. Vahdat, A., Ghasemi, B., Yousefpour, M., "Synthesis of hydroxyapatite and hydroxyapatite/Fe_3O_4 nanocomposite for removal of heavy metals", ***Environmental Nanotechnology, Monitoring & Management***, Vol 12, (2019), 100233-100238. https://doi.org/10.1016/j.enmm.2019.100233
5. Venkatesan, S., ul Hassan, M., Ryu, H. J., "Adsorption and immobilization of radioactive ionic-corrosion-products using magnetic hydroxyapatite and cold-sintering for nuclear waste management applications", ***Journal of Nuclear Materials***, Vol 514, (2019), 40-49. https://doi.org/10.1016/j.jnucmat.2018.11.026
6. Mondal, S., Manivasagan, P., Bharathiraja, S., Moorthy, M. S., Kim, H. H., Seo, H., Lee, K. D., Oh, J., "Magnetic hydroxyapatite: a promising multifunctional platform for nanomedicine application", ***International Journal of Nanomedicine***, Vol 12, (2017), 8389-8393. https://doi.org/10.2147/ijn.s147355
7. Zilm, M. E., Chen, L., Sharma, V., McDannald, A., Jain, M., Ramprasad, R., Wei, M., "Hydroxyapatite substituted by transition metals: experiment and theory", ***Physical Chemistry Chemical Physics***, Vol 18, No. 24, (2016), 16457-16465. https://doi.org/10.1039/c6cp00474a
8. Orooji, Y., Mortazavi-Derazkola, S., Ghoreishi, S. M., Amiri, M., Salavati-Niasari, M., "Mesopourous Fe_3O_4@ SiO_2-hydroxyapatite nanocomposite: Green sonochemical synthesis using strawberry fruit extract as a capping agent, characterization and their application in sulfasalazine delivery and cytotoxicity", ***Journal of Hazardous Materials***, Vol. 400, (2020), 123140. https://doi.org/10.1016/j.jhazmat.2020.123140
9. Katundi, D., Bayraktar, E., Gatamorta, F., Miskioglu, I., "Design of Hydroxyapatite/Magnetite (HAp/Fe_3O_4) Based Composites Reinforced with ZnO and MgO for Biomedical Applications", ***BiomedIcal Journal of Scientific & Technical Research***, Vol 21, No. 4, (2019), 16113. https://doi.org/10.26717/bjstr.2019.21.003649
10. Zeng, D., Dai, Y., Zhang, Z., Wang, Y., Cao, X., Liu, Y., "Magnetic solid-phase extraction of U(VI) in aqueous solution by Fe_3O_4@hydroxyapatite", ***Journal of Radioanalytical and Nuclear Chemistry***, Vol. 324, No. 3, (2020), 1329-1337. https://doi.org/10.1007/s10967-020-07148-y
11. Ain, Q. U., Zhang, H., Yaseen, M., Rasheed, U., Liu, K., Subhan, S., Tong, Z., "Facile fabrication of hydroxyapatite-magnetite-bentonite composite for efficient adsorption of Pb (II), Cd (II), and crystal violet from aqueous solution", ***Journal of Cleaner Production***, Vol 247, (2020), 119088. https://doi.org/10.1016/j.jclepro.2019.119088
12. Das, K. C., Dhar, S. S., "Remarkable catalytic degradation of malachite green by zinc supported on hydroxyapatite encapsulated magnesium ferrite (Zn/HAP/$MgFe_2O_4$) magnetic novel nanocomposite", ***Journal of Materials Science***, Vol 55, No. 11, (2020), 4592-4606. https://doi.org/10.1007/s10853-019-04294-x
13. Das, K. C., Das, B., Dhar, S. S., "Effective Catalytic Degradation of Organic Dyes by Nickel Supported on Hydroxyapatite-Encapsulated Cobalt Ferrite (Ni/HAP/$CoFe_2O_4$) Magnetic Novel Nanocomposite", ***Water, Air, & Soil Pollution***, Vol. 231, No. 2, (2020), 43. https://doi.org/10.1007/s11270-020-4409-1
14. Attia, M. A., Moussa, S. I., Sheha, R. R., Someda, H. H., Saad, E. A., "Hydroxyapatite/$NiFe_2O_4$ superparamagnetic composite: Facile synthesis and adsorption of rare elements", ***Applied Radiation and Isotopes***, Vol. 145, (2019), 85-94. https://doi.org/10.1016/j.apradiso.2018.12.003
15. Seyfoori, A., Ebrahimi, S. S., Omidian, S., Naghib, S. M., "Multifunctional magnetic $ZnFe_2O_4$-hydroxyapatite nanocomposite particles for local anti-cancer drug delivery and bacterial infection inhibition: an in vitro study", ***Journal of the Taiwan Institute of Chemical Engineers***, Vol. 96, (2019), 503-508. https://doi.org/10.1016/j.jtice.2018.10.018
16. Elkady, M., Shokry, H., Hamad, H., "Microwave-Assisted Synthesis of Magnetic Hydroxyapatite for Removal of Heavy Metals from Groundwater", ***Chemical Engineering & Technology***, Vol. 41, No. 3, (2018), 553-562. https://doi.org/10.1002/ceat.201600631
17. Sneha, M., Sundaram, N. M., "Preparation and characterization of an iron oxide-hydroxyapatite nanocomposite for potential bone cancer therapy", ***International Journal of Nanomedicine***, Vol 10, (2015), 99-105. https://doi.org/10.2147/ijn.s79985
18. Periyasamy, S., Gopalakannan, V., Viswanathan, N., "Hydrothermal assisted magnetic nano-hydroxyapatite encapsulated alginate beads for efficient Cr (VI) uptake from water", ***Journal of Environmental Chemical Engineering***, Vol. 6, No. 1, (2018), 1443-1454. https://doi.org/10.1016/j.jece.2018.01.007
19. Cullity, B. D., ***Elements of X-ray Diffraction***, 2nd Ed., edited by Morris Cohen, Addison-Wesley Publishing, (1977).
20. Younesi, M., Javadpour, S., Bahrololoom, M. E., "Effect of Heat Treatment Temperature on Chemical Compositions of Extracted Hydroxyapatite from Bovine Bone Ash", ***Journal of Materials Engineering and Performance***, Vol 20, No. 8, (2011) 1484-1490. https://doi.org/10.1007/s11665-010-9785-z
21. Xia, X., Chen, J., Shen, J., Huang, D., Duan, P., Zou, G., "Synthesis of hollow structural hydroxyapatite with different morphologies using calcium carbonate as hard template", ***Advanced Powder Technology***, Vol 29, No. 7, (2018), 1562-1570. https://doi.org/10.1016/j.apt.2018.03.021
22. Hamad, H. A., Abd El-latif, M. M., Kashyout, A. B., Sadik, W.A., Feteha, M.Y., "Study on synthesis of superparamagnetic spinel cobalt ferrite nanoparticles as layered double hydroxides by co-precipitation method", ***Russian Journal of General Chemistry***, Vol. 84, No. 10, (2014), 2031–2036. https://doi.org/10.1134/s1070363214100296
23. Sneha, M., Sundaram, N. M., "Preparation and characterization of an iron oxide-hydroxyapatite nanocomposite for potential bone cancer therapy", ***International Journal of Nanomedicine***, Vol 10, (2015), 99-106. https://doi.org/10.2147/ijn.s79985
24. Tien C., ***Adsorption Calculations and Modeling***, *Butterworth-Heinemann publisher*: Boston, (1994). https://doi.org/10.1016/c2009-0-26911-x
25. Atkinson, H. V., "Overview no. 65: Theories of normal grain growth in pure single phase systems", ***Acta Metallurgica***, Vol. 36, No. 3, (1988), 469-491. https://doi.org/10.1016/0001-6160(88)90079-x
26. Mobasherpour, I., Salahi, E., Manafi, S. A., Kamachali, R. D., "Effect of heat-treatment on grain growth of nanocrystalline tricalcium phosphate powder synthesized via the precipitation method", ***Materials Science-Poland***, Vol. 29, No. 3, (2011), 203-208. https://doi.org/10.2478/s13536-011-0032-6
27. Liu, F., Kirchheim, R., "Comparison between kinetic and thermodynamic effects on grain growth", ***Thin Solid Films***, Vol 466, No. 1-2, (2004), 108-113. https://doi.org/10.1016/j.tsf.2004.03.018
28. Höfler, H. J., Tao, R., Kim, L., Averback, R. S., Altstetter, C. J., "Mechanical properties of single-phase and nano-composite

metals and ceramics", ***Nanostructured Materials***, Vol. 6, No. 5-8, (1995), 901-904. https://doi.org/10.1016/0965-9773(95)00205-7

29. Liu, F., Kirchheim, R., "Nano-scale grain growth inhibited by reducing grain boundary energy through solute segregration", ***Journal of Crystal Growth***, Vol 264, No. 1-3, (2004), 385-391. https://doi.org/10.1016/j.jcrysgro.2003.12.021
30. Mobasherpour, I. Salahi, E., "Effect of heat treatment on grain growth of nanocrystalline hydroxyapatite powder", ***Journal of Ceramic Science and Technology***, Vol 2, No. 2, (2011), 119-124. https://doi.org/10.4416/JCST2010-00046